Luminescence dating of Late Pleistocene faults as evidence of uplift and active tectonics in Sardinia, W Mediterranean

Received: 15 October 2019 | Revised: 11 February 2020 | Accepted: 21 February 2020

DOI: 10.1111/ter.12458

RESEARCH ARTICLE

Terra Nova WILEY

Luminescence dating of Late Pleistocene faults as evidence of uplift and active tectonics in Sardinia, W Mediterranean

Leonardo Casini[1] | Stefano Andreucci[2] | Daniele Sechi[3] | Chun-Yuan Huang[4,5] | Chuan-Chou Shen[4,5] | Vincenzo Pascucci[3,6]

[1]Dipartimento di Chimica e Farmacia (DCF), Università di Sassari, Sassari, Italy

[2]Dipartimento di Scienze Chimiche e Geologiche (DiSCG), Università di Cagliari, Cittadella Universitaria di Monserrato, Cagliari, Italy

[3]Dipartimento di Architettura, Design e Urbanistica (DADU), Università di Sassari, Alghero, Italy

[4]High-Precision Mass Spectrometry and Environment Change Laboratory (HISPEC), Department of Geosciences, National Taiwan University, Taipei, Taiwan, ROC

[5]Research Center for Future Earth, National Taiwan University, Taipei, Taiwan, ROC

[6]Institute of Geology and Petroleum Technologies, Kazan Federal University, Kazan, Russia

Correspondence
Leonardo Casini, Dipartimento di Chimica e Farmacia (DCF), Università di Sassari, Via Piandanna 4, Sassari 07100, Italy.
Email: casini@uniss.it

Funding information
Ministry of Science and Technology, Grant/Award Number: 106-2628-M-002-013; National Taiwan University, Grant/Award Number: 105R7625; Ministry of Education, Grant/Award Number: 107L901001

Abstract

Precise dating of the activity of Late Pleistocene to Holocene neo-tectonic structures is crucial to quantify the rate of deformation in low-seismicity regions. Sardinia is a relatively stable continental fragment set in the middle of the tectonically active Western Mediterranean belt. This paper provides evidences of significant uplift of northwest Sardinia that support an ongoing tectonic activity since the Marine Isotopic Stage 7 (MIS 7; *ca.* 220 ka). In particular, it documents for the first time Late Pleistocene to Holocene tectonics based on luminescence dating of travertine sealing a major NNE-SSW fault.

1 | INTRODUCTION

Precise dating of Late Pleistocene to Holocene paleo-seismological records is crucial to detect neotectonic deformation, unmasking the long-term seismic behaviour of continental domains. The need for this information is even more crucial in low-seismicity regions characterized by long recurrence times in the range of 10^3 to 10^4 years or more (Ben-Zion, 2008; Scholz, 1968). However, it is often difficult to date neo-tectonic events, or even to find them in the geological record, because geomorphic features have very low preservation rate that yields to a systematic underestimation of the effective seismic potential (i.e., Leonard & Clark, 2011). A possible way for this drawback might be the use of Pleistocene marine markers (tidal notches, marine terraces, shallow marine deposits) and travertine. The first is not necessarily syntectonic deposits. However, because they mark the position of paleo-sea levels with little uncertainty, they are potential tracer of even minimal uplift or subsidence in coastal areas where can be used to derive fault slip-rates and Earthquake Recurrence Intervals (Muhs et al., 2014; Robertson, Meschis, Roberts, Ganas, & Gheorghiu, 2019; Rovere et al., 2016; Saillard et al., 2017; Santoro, Ferranti, Burrato, Mazzella, & Monaco, 2013).

Journal Name TER | Manuscript No. 12458 | WILEY | No. of pages: 11 | Dispatch: 3-3-2020 | PE: Yuvarani S. | CE: Prema

Travertines are continental carbonates that precipitate from deep CO_2-rich fluids pumped along crustal faults as long as the fractured zone remains permeable, which is only possible during tectonic activity or shortly after given the fast growth rate of these rocks (i.e., Brogi, Capezzuoli, Buracchi, & Branca, 2012; Hancock, Chalmers, Altunel, & Çakir, 1999; Kano et al., 2018; Özkul et al., 2013).

This paper provides compelling evidences to support neotectonics (Late Pleistocene to Holocene) in Sardinia, a low-seismicity continental fragment set in the middle of the western Mediterranean collisional belt (Figure 1).

Extensive luminescence dating of shallow-marine deposits correlative to late Middle and Late Pleistocene highstands evidenced post-MIS7 uplift and localized deformation accommodated by NNE and NW faults. The latest events could be as young as middle Holocene based on luminescence age dating of syntectonic travertine sealing a major NNE-SSW fault.

2 | GEODYNAMICS AND GEOLOGICAL SETTING

The western Mediterranean region has been interpreted as a segmented back-arc basin opened in response to lithospheric stretching during an eastward migration of the Apennines subduction zone (i.e., Cloetingh et al., 2005; Dewey, Helman, Knott, Turco, & Hutton, 1989; Doglioni, Gueguen, Harabaglia, & Mongelli, 1998; Jolivet & Faccenna, 2000). Overall, extension migrated eastward trough time from about 30 Ma yielding to the progressive opening of, from west to east, the Alboran, Balearic-Provençal basins and Tyrrhenian Sea (Figure 1), which has opened at a rate of about 30 to 50 mm/year (i.e., Faccenna, Becker, Lucente, Jolivet, & Rossetti, 2001). Geophysical constraints and kinematic models, based on GPS-data, however, indicate that Africa is still moving towards the stable Europe yielding to average N-S velocities between 3 to 15 mm/year (Faccenna et al., 2001; Serpelloni et al., 2007). The Corsica-Sardinia (C-S) block (Figure 1) separates the Balearic-Provençal basin from the Tyrrhenian Sea and represents a continental fragment detached in the Late Oligocene/Early Miocene from southern Europe. C-S block is characterized by a deeply incised topography with several peaks exceeding 2000 m above present sea level-a.p.s.l., a relatively thick crust in the interior (30–35 km), transitional margins (15–20 km) and a lithospheric mantle not exceeding a 60 km thickness (Finetti, 2005).

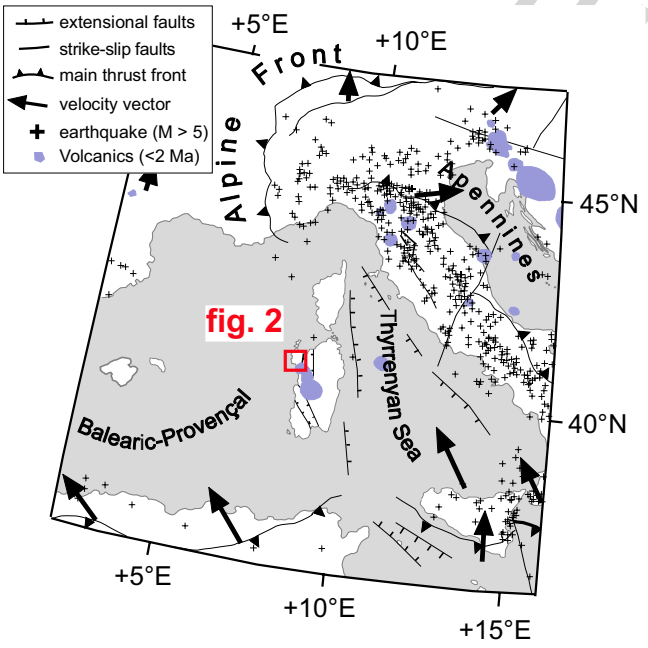

FIGURE 1 Structural sketch map of W Mediterranean, together with main seismic and Quaternary magmatic features of the region. The position in the study area is indicated by a black rectangle (Figure 2)

Most of the seismicity (peak magnitude in the range of Mw 5–8) observed in the W Mediterranean, together with Quaternary volcanism, is localized along the Alps and Apennines (Figure 1). Conversely, the C-S block is almost devoid of any appreciable historical seismicity and shows only a few compressional earthquakes (Mw <5) offshore of S Sardinia, plus other strike-slip or compressional in the N and NE sectors (Barhouni et al., 2013; Serpelloni et al., 2007; Vannucci & Gasperini, 2004). Moreover, the preservation of Marine Isotopic Stage 5e (MIS5e) marine markers in Sardinia, close to the mean global eustatic position (ca. 6 m a.p.s.l.), is commonly taken as an evidence for tectonic stability of the island, frequently used as a reference site to calibrate Quaternary sea-level fluctuations (i.e., Antonioli et al., 2017; Lambeck et al., 2011; Rovere et al., 2016). Nevertheless, the presence of several Middle-Upper Pleistocene marine markers above the present sea level along with rare and low magnitude earthquakes and high-resolution GPS dataset warn to a possible tectonic instability of Sardinia (Cocco, Andreucci, Sechi, Cossu, & Funedda, 2019; INGV, 2018).

The study area is located on the North-West Sardinia coast. It consists of a southern large bay (Porto Conte) bounded by two highs (~ 200 m a.p.s.l.) Punta Giglio and Capo Caccia promontories made of Mesozoic limestone (Figure 2). North and south of the bay, the coast is characterized by small coves and bays where incipient pocket sand and gravel beaches occur. The Quaternary strata drape Permo-Triassic sedimentary rocks, mainly quartz-rich sandstones and conglomerates (redbeds) and Triassic-Jurassic limestones/dolostones. Two sites, Cala Viola (cv) and Le Bombarde (bo) have been selected for this study because Quaternary strata and diffuse travertine encrustations are well preserved (Figure 2).

3 | METHODS

A detailed sedimentological analysis on the Quaternary successions of Cala Viola (cv) and Le Bombarde (bo) areas was performed to define the depositional environment on which these deposits developed. Second, the analysis of faults has been conducted on both outcrops and aerial/satellite images. Third, the main sedimentary bodies, as well as a travertine deposits, were dated using both quartz OSL and k-feldspar $pIRIR_{290}$ luminescence and U/Th-Pb methods. Dating has allowed us to define the stratigraphic position of the main sedimentary

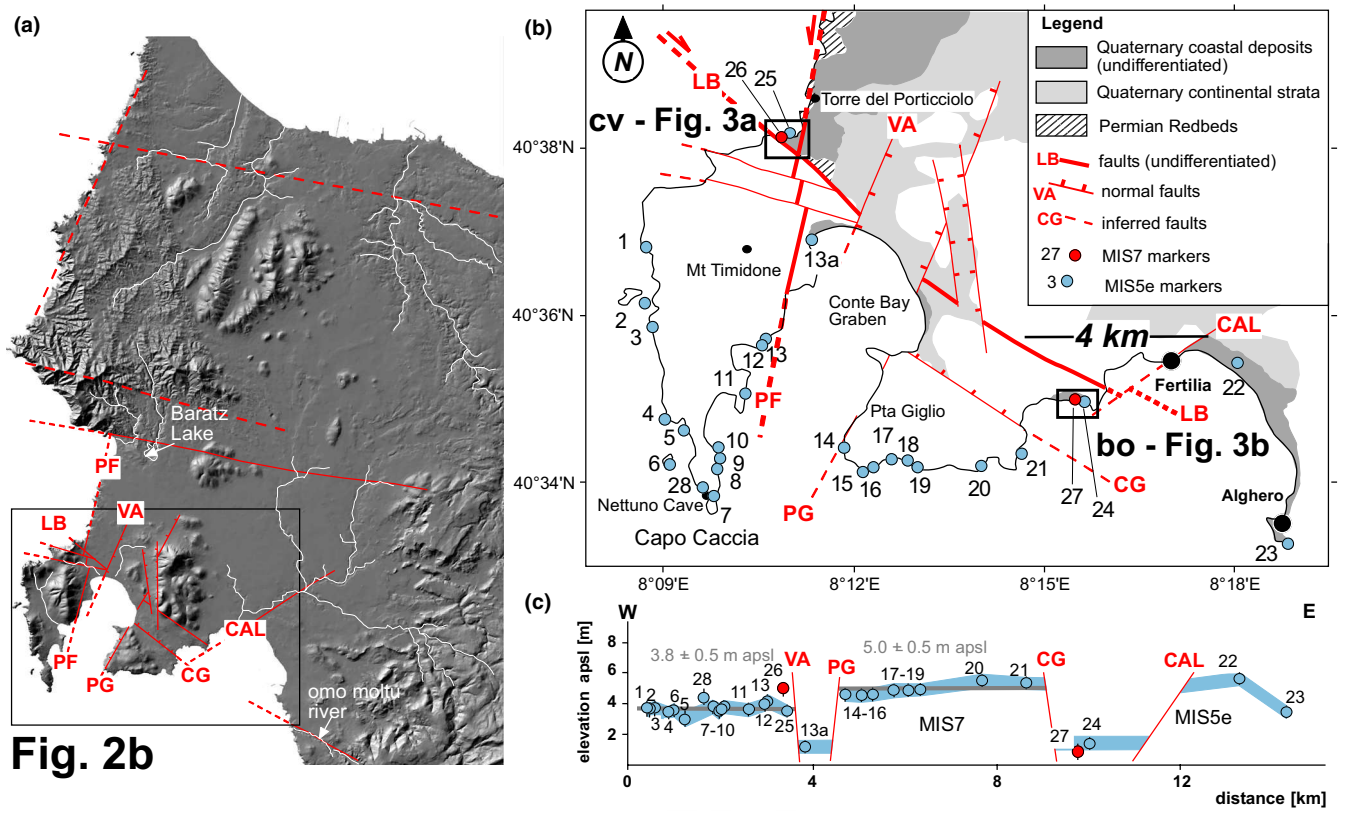

FIGURE 2 Simplified geological map of NW Sardinia, showing the main faults and Quaternary deposits. The black rectangles (Figure 3a,b) indicate the position of cv and bo sampling sites, respectively. Points numbered from 1 to 28 indicate the position of MIS5e (blue) and MIS7 sea-level markers (Table S2). The spatial variation of marker elevation a.p.s.l. is summarized below the map

bodies and marine terraces, the depositional age of travertine and, point out the sedimentary and tectonic evolution of the area through time. A brief discussion of the reliability of the derived ages is also presented (see Supporting Information). The transition shoreface-foreshore (or outerframe/sand run-fair weather berm sensu Pascucci, Martini, & Endres, 2009) is used as paleo sea-level marker because, in the Mediterranean Sea, normally placed at 0 ± 30 cm above the present sea level (Pascucci et al., 2018). The estimated paleo sea-level elevation is based on the equation provided by Rovere et al. (2016). These data have been compared with those published in the study area and referred to MIS5e: tidal notches (Ferranti et al., 2006; Palombo et al., 2017), coastal speleothems (Tuccimei et al., 2012), lagoon deposits (Zucca et al., 2014), algal build-up (Sechi et al., 2018) and shell layer (Ratto, Montis, Depalmas, Rendeli, & Melis, 2016).

4 | RESULTS

4.1 | Quaternary stratigraphy

In the selected cv (Figures 3 and 4) and bo (Figure 5) sites well-developed and preserved marine terraces are present. These deposits have been referred to as MIS7 and MIS5e interglacials on the basis of stratigraphic correlation and OSL age dating (Supporting Information). The studied MIS7 and MIS5e terraces are commonly associated to shallow-marine (shoreface and beachface) deposits accumulated in small pocket-beach systems.

In cv site MIS7 terrace lies on dune and or alluvial fan deposits referred to MIS8 (Figure 3b-e). It is composed of poorly sorted coarse conglomerates with few interlayered sands grading upward to plane-bedded sandstones and openwork pebbly conglomerate (Figure 3c-e). These deposits are interpreted as the outerframe (shoreface) and sand run-fair weather berm (beachface) of a coarse gravel pocket beach, respectively.

The MIS5e terrace lies on Permo-Triassic bedrock (Figures 3b and 4b). It is composed of well-sorted and well-rounded cobble to pebble conglomerates passing upward to plane laminated sandstones with diffuse open work pebbly layers (Figure 4a,c). This transition is interpreted as the boundary outerframe-sand run of a sand and gravel pocket beach.

In the bo site (Figure 5a) the MIS7 terrace lies on Mesozoic limestones (Figure 5b), and is composed of openwork, pebble and granule conglomerates with dispersed shells (entire and in fragments). It is interpreted as the fair-weather berm part of a gravelly pocket beach (Figure 5c,d).

The MIS5e terrace lies on MIS6 continental deposits SAR-OSL dated at 197 ± 41 (Pascucci at al., 2014) (Figure 5b). The marine deposit is composed of well-sorted low angle cross-laminated medium to coarse-grained sandstones with dispersed well-rounded pebbles

COLOUR online, B&W in print

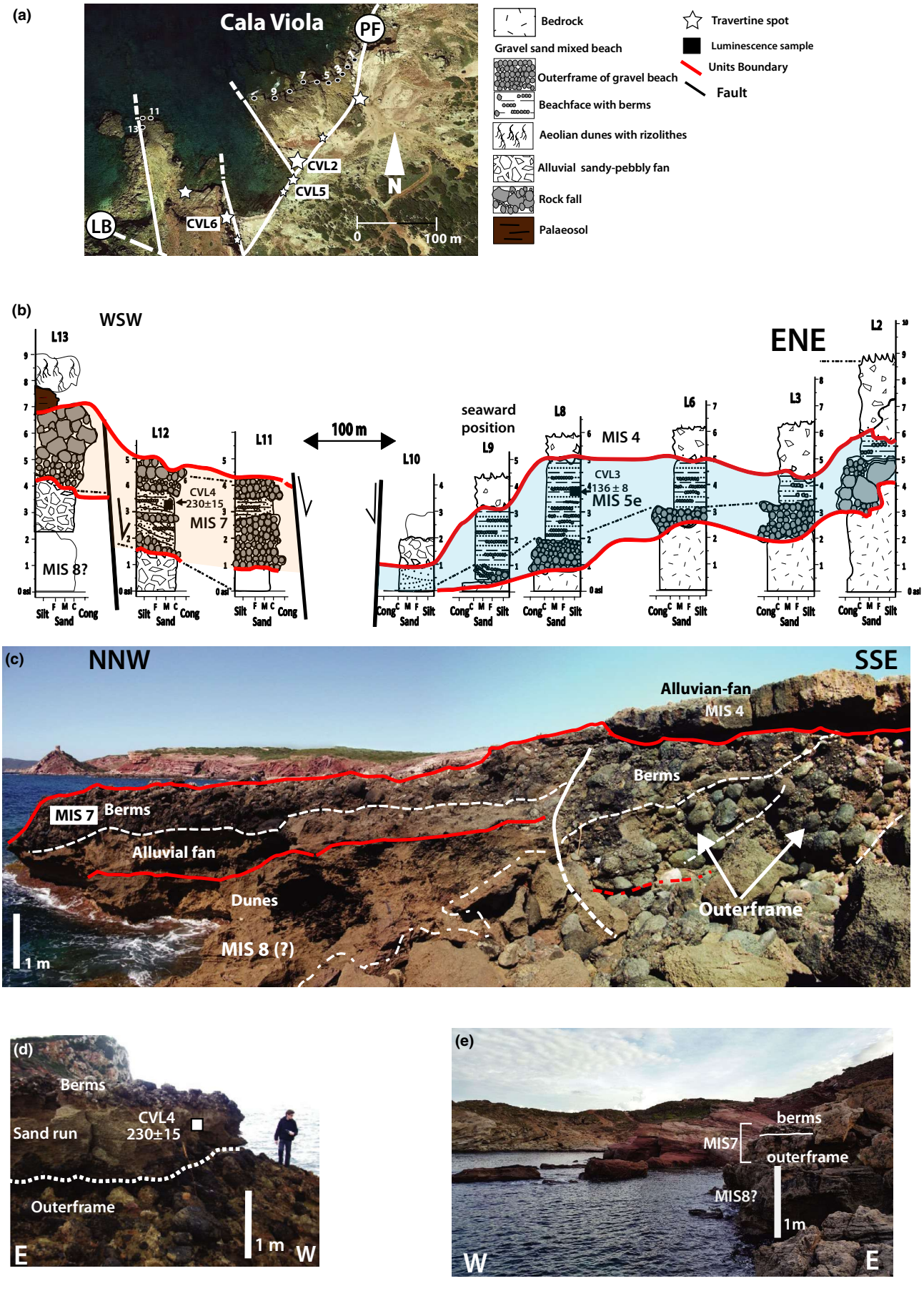

FIGURE 3 Field logs measured at Cala Viola (cv) site. (a) Location map of the logs and main faults. Progressive numbers indicate the position of logs according to labels of 3B; (b) Measured logs; (c) General view of the conglomerates composing MIS7 marine terrace. The outerframe (shoreface) and the berms are always indicated in the figure. (d) Location of sample CVL4 just above the boundary outerframe/sand run (shoreface-foreshore), log 12; (e) Lateral view of the MIS7 marine terrace (log 11). Ages are in ka (see Supporting Information for more details)

COLOUR online, B&W in print

FIGURE 4 Sedimentary facies characterizing deposits of MIS5 marine terrace. (a) Location of sample CVL3 immediately above the boundary outerframe/sand run (shoreface-foreshore); (b) Detail of the MIS5 marine terrace; (c) Close detail of the boundary outerframe/sand run. All ages are in ka and referred to SAR-OSL; that is, quartz (see Supporting Information for more details)

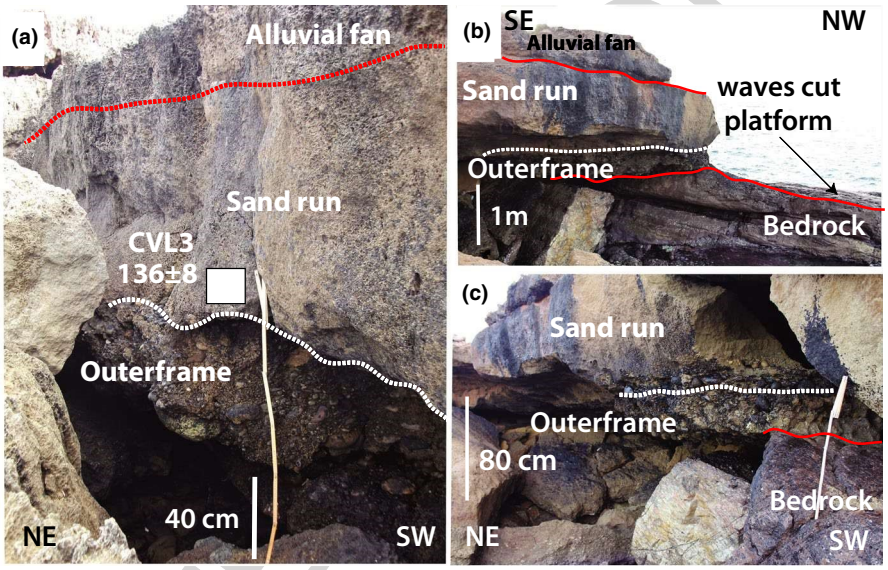

and shells (Figure 5e,f). These sandstones have been interpreted as the foreshore of a pocket sandy beach.

4.2 | Faults

Four are the major faults controlling the structural evolution of the studied area: Le Bombarde (LB), NW-SE oriented, Porto Ferro (PF), Villassunta (VA) and Punta Giglio (PG), these latter almost NNE-SSW oriented (Figure 2a,b).

The LB fault zone separates the Mesozoic platform carbonate, exposed in the Capo Caccia and Pta Giglio promontories (footwall), from the Paleozoic Permian redbeds and Quaternary sediments exposed in the plains between Torre del Porticciolo and Fertilia. The latter two faults (VA, PG) are roughly dip-slip and bound the Conte Bay graben (Figure 2b). Therefore, the studied paleo-beach systems are preserved in two fault-bounded triangular domains delimited by NW-SE and NNE-SSE conjugate faults (LB, PF, VA, PG; Figures 2a,b and 6a).

5 | GEOCHRONOLOGY

The ages of selected paleo-beach systems (Table 1) were determined by applying different luminescence protocols on both quartz (OSL) and k-feldspar (IR_{50}, $pIRIR_{290}$) grains (See Table S4). The beach system exposed towards the south of the bo site (sample BOM0, Figure 5), yield two undistinguishable luminescence ages (207 ± 20 and 205 ± 17 ka, Table 1) that confirms the inferred MIS7 age of this deposit. The alluvial fan capping both the MIS5e and MIS7 beach systems at bo site has an age of 83 ± 4 ka (BOM3, Figure 5; Table 1) and thus referred to MIS5a/4. At cv site, ages of the paleo-beach confirm their attribution to MIS7 (230 ± 14 ka, CVL4) and MIS5e (136 ± 8 ka, CVL3; Figure 3, see also Table S4).

Luminescence along with U/Th-Pb dating has been tentatively applied also to constrain the formation age of a syntectonic impure travertine mound precipitated just at the intersection between the LB and PF faults in the cv site (Figure 6b). Sample CVL2 gave two undistinguishable luminescence ages of 3.6 ± 0.2 and 3.7 ± 0.5 ka (Table 1). Two U/Th-Pb uncorrected ages (samples CVL5, CVL6) obtained along the same fault are 32.9 ± 6.5 ka and 31.5 ± 3.5 ka, respectively, supporting the Holocene age of travertine (Table 1). These U/Th-Pb ages have to be considered only as rough lower limit because of the diffuse presence of detrital Th in the system yield to severe aging (See Supporting Information) (Shen et al., 2003, 2012).

6 | ELEVATION OF PALEO-SEA LEVEL MARKERS

In the northern cv site, in the footwall of a minor fault parallel to LB, the outerframe-fairweather berm boundary of the MIS7 terrace is at 3.0 m a.p.s.l.(log 12, Figure 3). According to the equation provided by Rovere et al. (2016) the paleo Relative Sea Level (pRSL) is of 2.9 ± 0.2 m a.p.s.l. In the bo site the MIS7 beachface lies between 0

COLOUR online, B&W in print

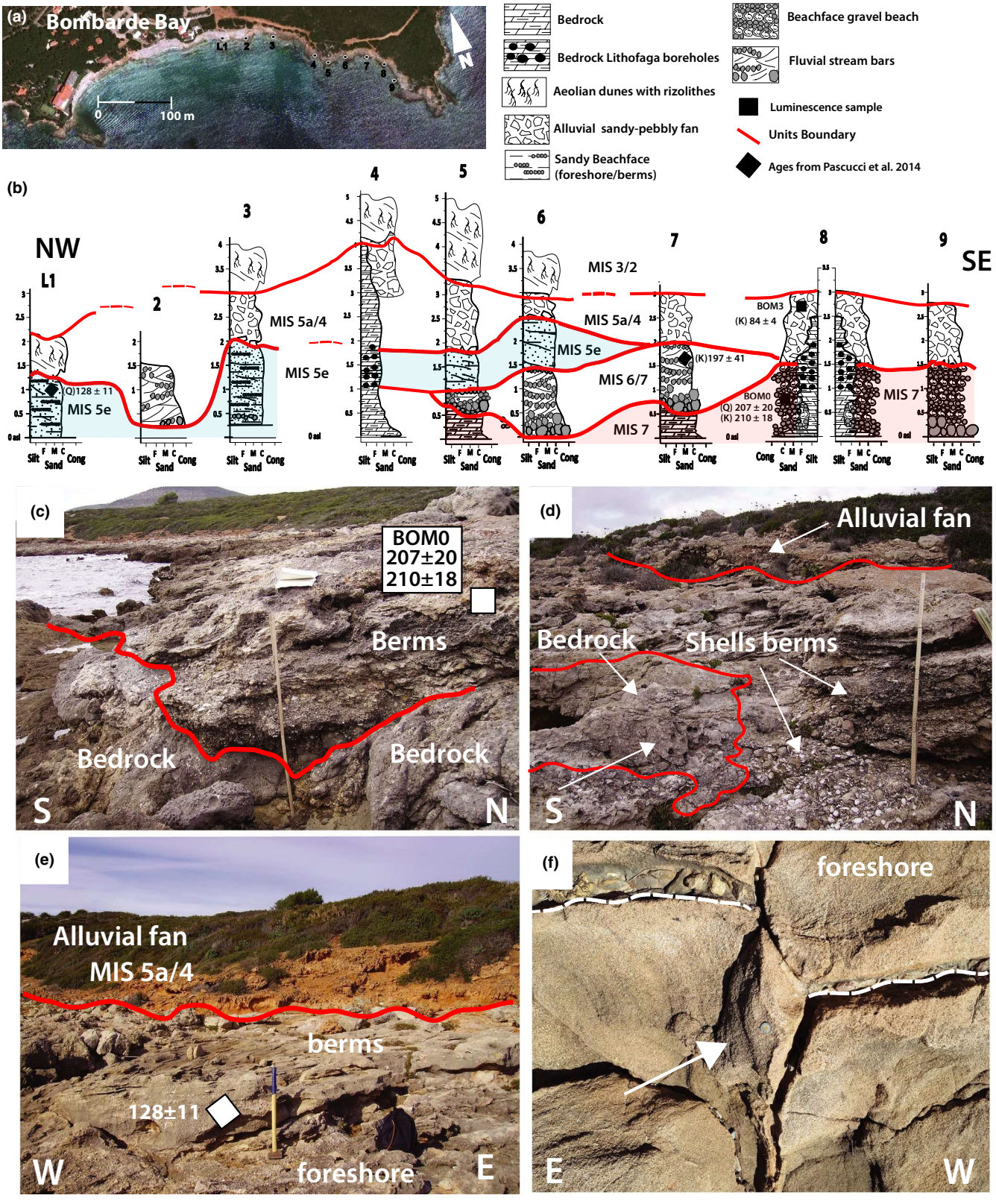

FIGURE 5 Field logs measured at Le Bombarde site (bo). (a) Location map of the logs and main faults. Progressive numbers indicate the position of logs according to labels of 5B; (b) Measured logs; (c) Location of sample BOM0 inside the berms (backshore), log 8; (d) Detail of the transition between MIS7 marine and MIS6 alluvial deposits (log 8); (e) Location of sample BOM3 and of Bombarde Bay 128 ± 11 (this last after Pascucci et al., 2014); (f) Detail of a fault cutting MIS5 marine terrace; note the several centimetres downthrown (arrow indicates 1€ for scale = 2 cm in diameter). All ages are in ka and referred to SAR-OSL; that is, quartz. When preceded by k are post- $pIRIR_{290}$ages; that is, k-feldspar (see Supporting Information for more details)

COLOUR online, B&W in print

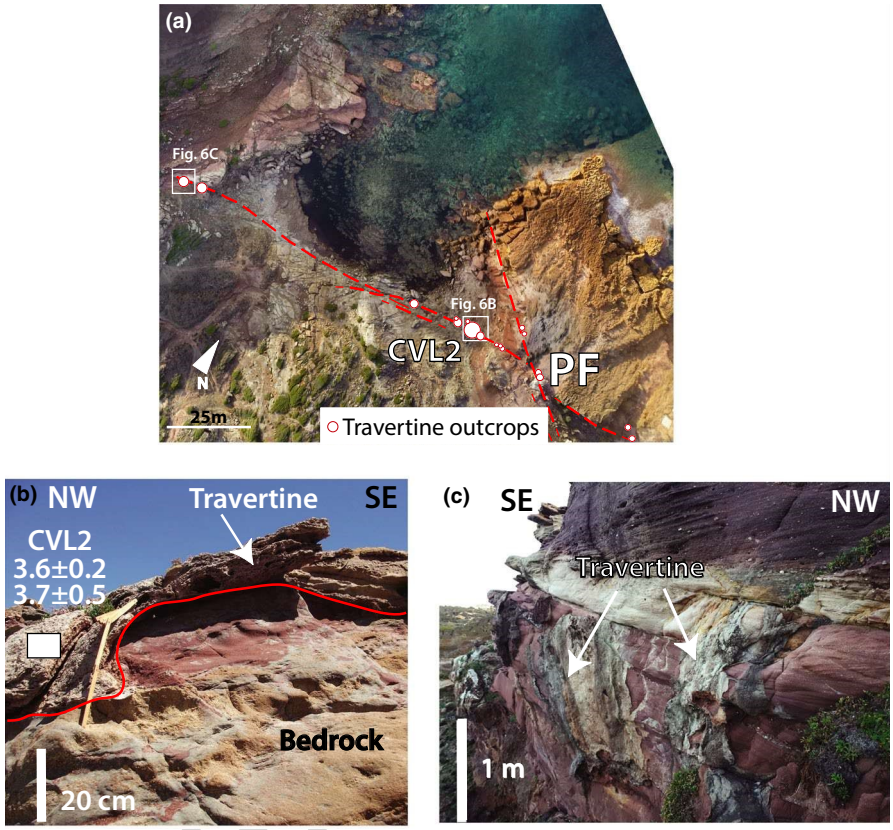

FIGURE 6 (a) Aerial view and location map of the travertine outcrops (red dots) and Porto Ferro (PF) fault at Cala Viola site (cv). Faults arrays are enhanced by light red colour. (b) Location of the samples CVL2. The derived ages of 3.6 ± 0.2 and 3.7 ± 0.5 are respectively referred to SAR-OSL (quartz) and IR_{50} (k-feldspar)and expressed in ka. (c) Details of travertine crust on the Porto Ferro (PF) fault

TABLE 1 Luminescence SAR-OSL (a) made on quartz grain; pIRIR290 and IRSL50 (b) made on k-feldspar grain, and U/Th absolute age dating

Deposits	Sample ID	Zs (m)	Zsh-fr (m)	Method	Age (ka)
Travertine	**CVL2**	—	—	SAR-OSL	**3.6 ± 0.2[a]**
				IR_{50}	**3.7 ± 0.5[b]**
Beachface	**CVL3**	**3.5**	**3**	SAR-OSL	105[a]
				IR_{50}	53 ± 4[b]
				$pIRIR_{290}$	**136 ± 8**
Beachface	**CVL4**	**3**	**2**	SAR-OSL	237[a]
				IR_{50}	92 ± 6[b]
				$pIRIR_{290}$	**230 ± 15**
Beachface	**BOM0**	**1.5**	**1**	SAR-OSL	207 ± 20
				IR_{50}	112 ± 8[b]
				$pIRIR_{290}$	**210 ± 18**
Colluvium	**BOM3**	**3**	—	SAR-OSL	60[a]
				IR_{50}	**70 ± 6**
				$pIRIR_{290}$	**84 ± 4**

Zs = the high of the sample above the present sea level; Zsh-fr = the high of the transition shoreface/foreshore above the present sea level.

and 1.5 m a.p.s.l. (log 4, 5, Figure 5) and thus the paleo Relative Sea Level (pRSL) is of 0.6 ± 1 m a.p.s.l.

In cv site, the highest shoreface-beachface boundary of MIS5e beach system has a mean elevation of 3.5 m a.p.s.l. and crops out in the hanging wall of the LB fault (logs9-3, Figure 3). The pRSL is of 3.4 ± 0.2 m a.p.s.l. At the bo site, the foreshore crops out between 0 and 2.5 m a.p.s.l. (log 1–6, Figure 5b)., thus, the pRSL is of 1.1 ± 1.5 m a.p.s.l.

Along the steep Mesozoic limestone cliffs bounding Capo Caccia promontory and the north side of the Conte Bay, paleo-tidal notches attributed to MIS5e are exposed at an average elevation of 3.8 ± 0.5 m a.p.s.l. (1–13 of Figure 2; Ferranti et al., 2006) in agreement with the speleothem of Nettuno cave +4.3 m a.p.s.l. (Tuccimei et al., 2012). The average elevation of the notch around Pta Giglio promontory is, instead 5 ± 0.5 m a.p.s.l. (14–21 Figure 2; Palombo et al., 2017) (see Table S1).

7 | DISCUSSION AND CONCLUSIONS

Recent high-resolution DGPS measurements evidenced a major variability of vertical velocities along the western coast of the island. Here, few sites record localized uplift at moderate rates (1.6 ± 0.6–1.0 ± 0.3 mm/year; Antonioli et al., 2017); yet, the general trend of the island is consistent with low subsidence (0.01 mm/year; Ferranti et al., 2006). The mean position of MIS7c beach systems is globally placed between −27 and −2.5 m below the present sea level (Grant et al., 2014; Waelbroeck et al., 2002; Woodroffe & Webster, 2014) (Figure 7). Thus, extrapolating the inferred mean subsidence rates of Sardinia, MIS7 marine terraces should be presently submerged between −30 and −5 m. The persistence of these terraces above the present sea level (from 0 to +5 m a.p.s.l.; Figures 3 and 5) indicates that the western coast of Sardinia records, at least locally, a significant uplift (35–10 m) lasting until about 130 ka (Figure 8). Uplift apparently stops or migrated by the following interglacial as MIS5e highstands are mostly close to their expected eustatic position (Figure 8). These observations, together with the metrical offset of MIS5e marine terraces provide substantial evidence for vertical movements accommodated by post MIS7 to Holocene faulting, as summarized in the conceptual model of Figure 8.

Although the vertical displacement of MIS5e markers is relatively small (1–5 m, Figure 2c) it is significant because it exceeds the uncertainty of both stratigraphic and luminescence dating methods. Moreover, the elevation of MIS5e markers evidences several short wavelength (1–10 km) oscillations that cannot fit any simplistic model of regional-scale differential subsidence, suggesting the existence of several fault-bounded domains recording differential vertical movements (Figure 2c).

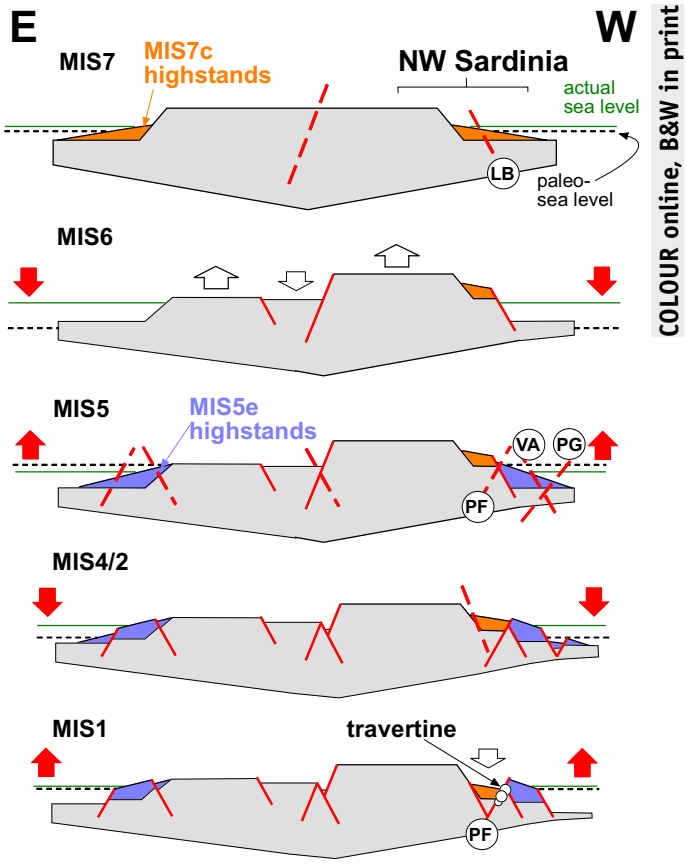

FIGURE 8 Conceptual model for post-MIS7 tectonic activity in NW Sardinia (not to scale). The green line marks the position of the actual sea level. The black dashed lines denote paleo-sea level at different snapshots. Red arrows indicate the rise/fall of water table, white arrows denote uplift/subsidence patterns. The main faults are indicated as red lines (dashed lines for activating faults); fault labels as explained in the text and Figure 2

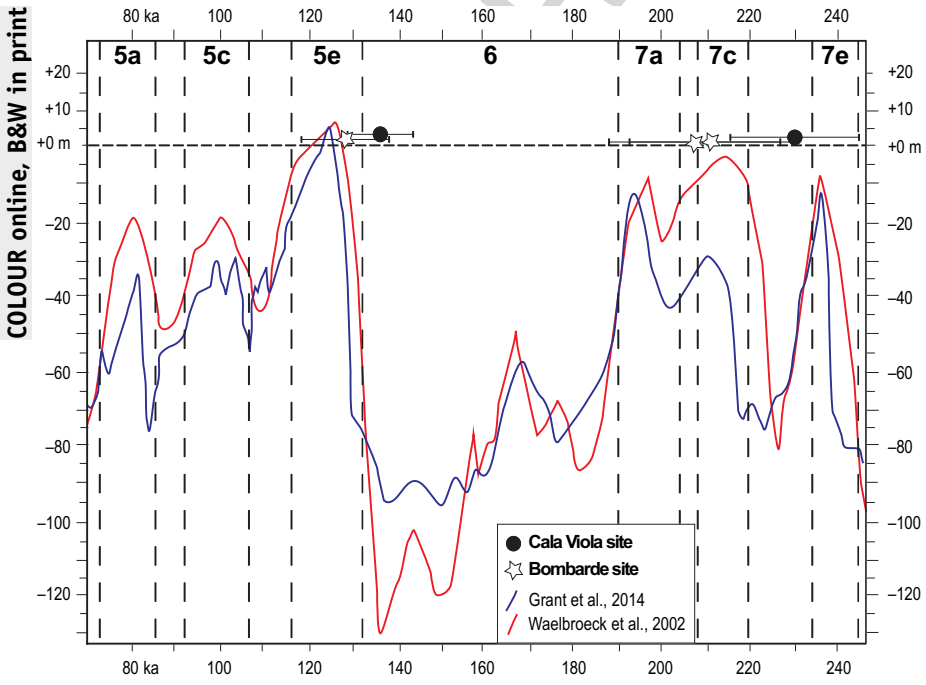

FIGURE 7 Cala Viola (black dots) and Le Bombarde (stars) beach ages plotted on the mean sea level curves by Waelbroeck et al. (2002) (red curve) and Grant et al. (2014) (blue curve)

Presently, the major faults strike roughly N-S and NW-SE, respectively, and are thus favorably oriented for reactivation as extensional faults (Figure 1). Yet, it is likely that MIS5e markers capture only a fraction of recent deformation as large extensional displacements would have taken marine terraces underwater. All these features argue for recent, though slow, deformation and cannot be reconciled with the paradigm of tectonic stability (Figure 8). The alternative is to admit that the latest interglacials are characterized by unrecognized high-frequency oscillations, which are below the sensitivity of luminescence.

Moreover, precise luminescence dating of Holocene travertine sealing a post-MIS5e fault is documented for the first time in Sardinia. This demonstrates a previously unrecognized neo-tectonic activity that should be accounted for in the future revisions of geodynamic models. The results of this work also demonstrate the applicability of luminescence to precisely date impure travertines complementing the U-Th method.

ACKNOWLEDGEMENTS

This research has been granted by Base Research Project, L.R. 7 agosto 2007, Project: "Cambiamenti climatici e neotettonica – la Sardegna un continente semi-stabile", founded by Regione Autonoma della Sardegna, (RAS, Assessorato della Programmazione, Bilancio, Credito e Assetto del Territorio - Code RAS SR14473 - Bando 2017, Resp. Vincenzo Pascucci). It also benefits of a partial support by the Science Vanguard Research Program of the Ministry of Science and Technology (MOST) (106-2628-M-002-013 to C.-C.S.), the National Taiwan University (105R7625 to C.-C.S.), the Higher Education Sprout Project of the Ministry of Education, Taiwan ROC (107L901001 to C.-C.S.).

DATA AVAILABILITY STATEMENT

The authors confirm that the data supporting the findings of this study are available within the article and its Supporting Information.

ORCID

Leonardo Casini https://orcid.org/0000-0002-6157-1865
Stefano Andreucci https://orcid.org/0000-0001-8073-5354

REFERENCES

Andreucci, S., Clemmensen, L. B., Murray, A., & Pascucci, V. 2010. Middle to late Pleistocene coastal deposits of Alghero, northwest Sardinia (Italy): Chronology and evolution. *Quaternary International*. *222*(1-2), 3–16. https://doi.org/10.1016/j.quaint.2009.07.025

Andreucci, S., Clemmensen, L. B., & Pascucci, V. (2010). Transgressive dune formation along a cliffed coast, NW Sardinia (Italy): A record of Late Pleistocene climate change. In V. Pascucci (Ed.), *Late Pleistocene response to climate change and sea level variation* (Vol. 22, pp. 424–433). Oxford, UK: Terra Nova.

Andreucci, S., Sechi, D., Buylaert, J. P., Sanna, L., & Pascucci, V. (2017). Post-IR IRSL290 dating of K-rich feldspar sand grains in a wind-dominated system on Sardinia. *Marine and Petroleum Geology*, *87*, 91–98. https://doi.org/10.1016/j.marpetgeo.2017.03.025

Antonioli, F., Anzidei, M., Amorosi, A., Lo Presti, V., Mastronuzzi, G., Deiana, G., … Vecchio, A. 2017. Sea-level rise and potential drowning of the Italian coastal plains: flooding risk scenarios for 2100. *Quaternary Science Reviews*, *158*, 29–43. https://doi.org/10.1016/j.quascirev.2016.12.021

Antonioli, F., Ferranti, L., & Kershaw, S. (2006). A glacial isostatic adjustment origin for double MIS 5.5 and Holocene marine notches in the coastline of Italy. *Quaternary International*, *145-146*, 19–29. https://doi.org/10.1016/j.quaint.2005.07.004

Bahrouni, N., Bouaziz, S., Soumaya, A., Ben Ayed, N., Attafi, K., Houla, Y., … Rebai, N. (2014). Neotectonic and seismotectonic investigation of seismically active regions in Tunisia: A multidisciplinary approach. *Journal of Seismology*, *18*, 235–256. https://doi.org/10.1007/s10950-013-9395-y

Ben-Zion, Y. (2008). Collective behavior of earthquakes and faults: Continuum-discrete transitions, progressive evolutionary changes, and different geodynamic regimes. *Reviews of Geophysics*. *46*, RG4006. https://doi.org/10.1029/2008RG000260

Brogi, A., Capezzuoli, E., Buracchi, E., & Branca, M. (2012). Tectonic control on travertineand calcareous tufa deposition in a low-temperature geothermal system (Sarteano. Central Italy). *Journal of Geological Society*, *169*, 461–476. https://doi.org/10.1144/0016-76492011-137

Cheng, H., Edwards, R. L., Shen, C.-C., Polyak, V. J., Asmerom, Y., Woodhead, J., … Spötl, C. (2013). Improvements in ^{230}Th dating, ^{230}Th and ^{234}U half-life values, and U-Th isotopic measurements by multi-collector inductively coupled plasma mass spectroscopy. *Earth and Planetary Science Letters*, *371–372*. 82–91.

Cloetingh, S., Ziegler, P. A., Beekman, F., Andriessen, P. A. M., Matenco, L., Bada, G., … Sokoutis, D. 2005. Lithospheric memory, state of stress and rheology: neotectonic controls on Europe's intraplate continental topography. *Quaternary Science Reviews*, *24*(3-4), 241–304.

Cocco, F., Andreucci, S., Sechi, D., Cossu, G., & Funedda, A. (2019). Upper Pleistocene tectonics in western Sardinia (Italy): Insights from the Sinis peninsula structural high. *Terra Nova*, *31*, 485–493. https://doi.org/10.1111/ter.12418

Dewey, J. F., Helman, M. L., Knott, S. D., Turco, E., & Hutton, D. H. W.1989. Kinematics of the western Mediterranean. In M. P. Coward, D. Dietrich, & R. G. Park (Eds.), *Alpine tectonics*, (Vol. 45, pp. 265–283). London, UK: Geological Society London Special Publications.

Doglioni, C., Gueguen, E., Harabaglia, P., & Mongelli, F.1998. On the origin of W-directed subduction zones and applications to the western Mediterranean. In B. Durand, L. Jolivet, F. Horvath, & M. Séranne (Eds.), *The Mediterranean basins: Tertiary extension within the Alpine Orogen*, (Vol. 156, pp. 541–561). London, UK: Geological Society London Special Publication.

Faccenna, C., Becker, T. W., Lucente, F. P., Jolivet, L., & Rossetti, F. 2001. History of subduction and back-arc extension in the Central Mediterranean. *Geophysical Journal International*, *145*(3), 809–820. https://doi.org/10.1046/j.0956-540x.2001.01435.x

Ferranti, L., Antonioli, F., Mauz, B., Amorosi, A., Dai Pra, G., Mastronuzzi, G., … Verrubbi, V. 2006. Markers of the last interglacial sea-level high stand along the coast of Italy: tectonic implications. *Quaternary International*, *145-146*, 30–54. https://doi.org/10.1016/j.quaint.2005.07.009

Grant, K. M., Rohling, E. J., Bronk Ramsey, C., Cheng, H., Edwards, R. L., Florindo, F., … Williams, F. 2014. Sea-level variability over five glacial cycles. *Nature Communications*, *5*(1), 50–76. https://doi.org/10.1038/ncomms6076

Grünthal, G., Wahlström, R., & Stromeyer, D. (2009). The unified catalogue of earthquakes in central, northern, and northwestern Europe (CENEC) - updated and expanded to the last millennium. *Journal of Seismology*, *13*, 517–541. https://doi.org/10.1007/s10950-008-9144-9

Hancock, P. L., Chalmers, R. M. L., Altunel, E., & Çakir, Z. 1999. Travitonics: Using travertines in active fault studies. *Journal of Structural Geology*. *21*(8-9), 903–916. https://doi.org/10.1016/S0191-8141(99)00061-9

INGV (2018). Catalogo parametrico dei terremoti italiani. Retrieved from https://emidius.mi.ingv.it/CPTI15-DBMI15/

Jolivet, L., & Faccenna, C. 2000. Mediterranean extension and the Africa-Eurasia collision. *Tectonics*, *19*(6), 1095–1106. https://doi.org/10.1029/2000TC900018

Lambeck, K., Antonioli, F., Anzidei, M., Ferranti, L., Leoni, G., Scicchitano, G., & Silenzi, S. 2011. Sea level change along the Italian coast during the Holocene and projections for the future. *Quaternary International*, *232*(1-2), 250–257. https://doi.org/10.1016/j.quaint.2010.04.026

Leonard, M., & Clark, D. 2011. A record of stable continental regions earthquakes from Western Australia spanning the late Pleistocene: Insights for contemporary seismicity. *Earth and Planetary Science Letters*, *309*, 207–212. https://doi.org/10.1016/j.epsl.2011.06.035

Muhs, D. R., Simmons, K. R., Schumann, R., Groves, L. T., De Vogel, S. T., Minor, S. A., & Laurel, D. (2014). Coastal tectonics on the eastern margin of the Pacific Rim: Late Quaternary sea-level history and uplift rates, Channel Islands National Park, California, USA. *Quaternary Science Reviews*, *105*, 209–238. https://doi.org/10.1016/j.quascirev.2014.09.017

Özkul, M., Kele, S., Gökgöz, A., Shen, C. C., Jones, B., Baykara, M. O., … Alçiçek, M. C. 2013. Comparison of the quaternary travertine sites intheDenizli extensional basin based on their depositional and geochemical data. *Sedimentary Geology*, *294*, 179–204. https://doi.org/10.1016/j.sedgeo.2013.05.018

Palombo, M. R., Antonioli, F., Lo Presti, V., Mannino, M. A., Melis, R. T., Orrù, P., … Altamura, S. 2017. The late Pleistocene to Holocene palaeogeographic evolution of the Porto Conte area: Clues for a better understanding of human colonization of Sardinia and faunal dynamics during the last 30 ka. *Quaternary International*, *439*, 117–140.

Pascucci, V., De Falco, G., Del Vais, C., Melis, R. T., Sanna, I., & Andreucci, S. 2018. Climate changes and human impact on the Mistras coastal barrier system (W Sardinia, Italy). *Marine Geology*, *395*, 271–284. https://doi.org/10.1016/j.margeo.2017.11.002

Pascucci, V., Martini, I. P., & Endres, A. (2009). Facies and Ground-penetrating-radar (GPR) characteristics of coarse-grained beach deposits of the uppermost Pleistocene glacial Lake Algonquin. *Ontario Canada: Sedimentology*, *56*, 529–545.

Pascucci, V., Sechi, D., & Andreucci, S. (2014). Middle Pleistocene to Holocene coastal evolution of NW Sardinia (Mediterranean Sea, Italy). *Quaternary International*, *328-329*, 3–20. https://doi.org/10.1016/j.quaint.2014.02.018

Ratto, G., Montis, F., Depalmas, A., Rendeli, M., & Melis, R. T. (2016). Paleoenvironmental reconstructionof the Sant'Imbenia area during the Middle Holocene (Sardinia, Italy). *Geografia Fisica Dinamica Quaternario*, *39*, 193–202. https://doi.org/10.4461/gfdq2016.39.18

Robertson, J., Meschis, M., Roberts, G. P., Ganas, A., & Gheorghiu, D. M. (2019). Temporally constant quaternary uplift rates and their relationship with extensional upper-plate faults in south crete (Greece), constrained with ^{36}Cl cosmogenic exposure dating. *Tectonics*, *38*, 1189–1222. https://doi.org/10.1029/2018TC005410

Rovere, A., Raymo, M. E., Vacchi, M., Lorscheid, T., Stocchi, P., Gómez-Pujol, L., … Hearty, P. J. (2016). The analysis of Last Interglacial (MIS 5e) relative sea-level indicators: Reconstructing sea-level in a warmer world. *Earth Sciences Reviews*, *159*, 404–427. https://doi.org/10.1016/j.earscirev.2016.06.006

Saillard, M., Audin, L., Rousset, B., Avouac, J.-P., Chlieh, M., Hall, S. R., … Farber, D. L. (2017). From the seismic cycle to long-term deformation: Linking seismic coupling and quaternary coastal geomorphology along the Andean Megathrust. *Tectonics*, *36*, 241–256. https://doi.org/10.1002/2016TC004156

Santoro, E., Ferranti, L., Burrato, P., Mazzella, M. E., & Monaco, C. (2013). Deformed Pleistocene marine terraces along the ionian Sea Margin of southern Italy: Unveiling blind fault-related folds contribution to coastal uplift. *Tectonics*, *32*, 737–762. https://doi.org/10.1002/tect.20036

Scholz, C. H. (1968). The frequency-magnitude relation of microfracturing in rock and its relation to earthquakes. *Bulletin of the Seismological Society of America*, *58*, 399–415.

Serpelloni, E., Vannucci, G., Pondrelli, S., Argnani, A., Casula, G., Anzidei, M., … Gasperini, P. (2007). Kinematics of the western Africa-Eurasia plate boundary from focal mechanisms and GPS data. *Geophysical Journal International*, *169*, 1180–1200. https://doi.org/10.1111/j.1365-246X.2007.03367.x

Shen, C.-C., Cheng, H., Edwards, R. L., Moran, S. B., Edmonds, H. N., Hoff, J. A., & Thomas, R. B. 2003. Measurement of attogram quantities of 231Pa in dissolved and particulate fractions of seawater by isotope dilution thermal ionization mass spectroscopy. *Analytical Chemistry*, *75*, 1075–1079.

Shen, C.-C., Wu, C.-C., Cheng, H., Edwards, R. L., Hsieh, Y.-T., Gallet, S., … Spötl, C. 2012. High-precision and high-resolution carbonate 230Th dating by MC-ICP-MS with SEM protocols. *Geochimica Et Cosmochimica Acta*, *99*, 71–86. https://doi.org/10.1016/j.gca.2012.09.018

Simms, A. R., Rouby, H., & Lambeck, K. (2016). Marine Terraces and Rates of Vertical Tectonic Motion: The Importance of glacio-isostatic Adjustment along the Pacific Coast of Central North America. *Geological Society of America Bulletin*, *128*, 81–93. https://doi.org/10.1130/B31299.1

Tuccimei, P., Onac, B. P., Dorale, J. A., Ginés, J., Fornós, J. J., Ginés, A., … Mucedda, M. 2012. Decoding last interglacial sea-level variations in the western Mediterranean using speleothem encrustations from coastal caves in Mallorca and Sardinia: A field data - model comparison. *Quaternary International*, *262*, 56–64. https://doi.org/10.1016/j.quaint.2011.10.032

Vannucci, G., & Gasperini, P. (2004). The new release of the database of earthquake mechanisms of the Mediterranean area (EMMA version 2). *Annals of Geophysics*, *47*, 307–334.

Waelbroeck, C., Labeyrie, L., Michel, E., Duplessy, J. C., McManus, J. F., Lambeck, K., … Labracherie, M. (2002). Sea-level and deep water temperature changes derived from benthic foraminifera isotopic records. *Quaternary Science Reviews*, *21*, 295–305. https://doi.org/10.1016/S0277-3791(01)00101-9

Woodroffe, C. D., & Webster, J. M. (2014). Coral reefs and sea-level change. *Marine Geology*, *352*, 248–267. https://doi.org/10.1016/j.margeo.2013.12.006

Zucca, C., Sechi, D., Andreucci, S., Shaddad, S. H., De Roma, M., Madrau, S., … Kapur, S. 2014. Pedogenic and palaeoclimatic evidence from an Eemian calcrete in North-western Sardinia (Italy). *European Journal of Soil Science*, *65*, 420–435. https://doi.org/10.1111/ejss.12144

SUPPORTING INFORMATION

Additional supporting information may be found online in the Supporting Information section.

Figure S1. Quartz luminescence characteristics: (a) pre-heat plateau test for sample CVL2: white circles show weak plateau between 200°C-260°C. Grey circles show the thermal transferred dose measured as function of thermal treatment after artificial bleaching of the signal. The inset shows the behaviour of recycling for the two tests. (b) Dose recovery pre-heat plateau test for sample CVL3 and BOM0. The dashed lines denote 10% of uncertainty. (c–e) Sensitivity dose response curves for sample CVL2, CVL3 and BOM0, respectively. (f) Distribution of recycling ratio for sample CVL2 dashed lines highlight the limit values of rejection

Figure S2. Feldspar luminescence characteristics: (a) dependency of pIRIR290 De on first IR temperature stimulation for samples CVL3 and BOM0. (b) Post-IR IRSL intensity and shape of decay curve performed at 290°C of stimulation; the inset shows the sensitivity corrected growth curve for CVL3 and BOM0 samples and the estimated Natural De. (c) Dependency of IR50 on preheating temperatures. (d) Decay curve of IR50, the inset shows the sensitivity corrected growth curve and interpolated Natural De

Figure S3. De distributions of cala viola (CVL) samples: probability density and radial plots. The red diamonds of probability distribution and the lines of radial plot were positioned at the CAM (Central Age Model, Galbraith et al., 1999; 2012). (a) SAR-OSL, (b) SAR-IR50 of CLV2. (c and d) pIRIR290 distribution of sample CVL3 and CVL4

Figure S4. De distribution of Le Bombarde sample (BOM) probability density and radial plots

Table S1. Late-Pleistocene sea-level markers used to define the MIS 5e and MIS 7 palaeo sea-level position

Table S2. Dose measurements protocols used in this study. SAR-OSL protocol after Murray and Wintle (2000, 2003), pIRIR290 developed after Thiel et al. (2011). For 'natural' sample, the given dose = 0. The whole sequence is repeated for several regenerative doses including zero dose and repeat dose (recuperation and recycling). For SAR-IR50 De steps 3 and 7 were used. Note that the pre-heat temperature used for sample CVL2 was 180°C

Table S3. Summary of samples characteristics, radionuclide concentrations, and derived quartz and feldspar doses. Depth = distance of sample from the surface; GS = grain-size used for luminescence analysis; WC = water content; Q-Dr; Kf int Dr = K-feldspar internal dose rate contribution to the total; Tot Kf-Dr

Table S4. Luminescence results

Table S5. Table of U/Th uncorrected ages

Data S1. xxxx

How to cite this article: Casini L, Andreucci S, Sechi D, Huang C-Y, Shen C-C, Pascucci V. Luminescence dating of Late Pleistocene faults as evidence of uplift and active tectonics in Sardinia, W Mediterranean. *Terra Nova*. 2020;00:1–11. https://doi.org/10.1111/ter.12458